

# Modeling the unsteady aerodynamic forces on small-scale wings

Steven L. Brunton\*, Clarence W. Rowley†

*Princeton University, Princeton, NJ 08544*

The goal of this work is to develop low order dynamical systems models for the unsteady aerodynamic forces on small wings and to better understand the physical characteristics of unsteady laminar separation. Reduced order models for a fixed, high angle of attack flat plate are obtained through Galerkin projection of the governing Navier-Stokes equations onto POD modes. Projected models are compared with direct numerical simulation (DNS) to show that they preserve qualitative behavior such as coherent structures. It is shown that in flows with Reynolds number 100, even a two degree of freedom model is sufficient to capture high angle of attack laminar vortex shedding. Next, the classical theories of Theodorsen and Wagner are compared with DNS for a number of pitch and plunge maneuvers of varying Strouhal number, reduced frequency, pitch amplitude and center. In addition to determining when these theories break down, the flow field structures are investigated to determine how the theories break down. This is an important first step toward combining and extending classical unsteady aerodynamic models to include high angle of attack effects. Theodorsen's model for the lift of a sinusoidally pitching or plunging plate is shown to agree moderately well with DNS for reduced frequencies  $k < 2.0$ . One major observation is that the classical aerodynamic models all begin to disagree when the effective angle of attack, either determined by Strouhal number in the plunging case or angle of attack excursion in the pitching case, exceeds the critical stall angle where vortex shedding and laminar separation become prominent. Velocity field and body force data for a flat plate are generated by 2D direct numerical simulation using an immersed boundary method for Reynolds number 100-300, and regions of separated flow and wake structures are visualized using Finite Time Lyapunov Exponents (FTLE) fields, the ridges of which are Lagrangian coherent structures (LCS).

## I. Introduction

Understanding the unsteady fluid dynamics associated with flow over small-scale wings has gained significant attention recently, both to study bird and insect flight as well as to develop advanced aerodynamic models for high-performance micro-aerial vehicles (MAVs). The short time scales involved in gusts and agile maneuvering make small wings susceptible to unsteady laminar separation, which can either enhance or destroy the lift depending on the specific maneuver and extent of flow control authority. For example, certain insects<sup>1-3</sup> and birds<sup>4</sup> use the shape and motion of their wings to maintain the high transient lift associated with a rapid pitch-up, while avoiding stall and the substantially decreased lift which follows. Dynamic stall occurs when the effective angle of attack changes rapidly so that a leading-edge vortex forms, provides temporarily enhanced lift and decreased pitching moment, and then sheds downstream, resulting in stall.<sup>5</sup> This phenomenon is well known in the rotorcraft community<sup>6</sup> since it is necessary to pitch the blades down as they advance and pitch up as they retreat to balance lift in forward flight. The potential performance gains observed in bio-locomotion make this an interesting problem for model-based control in the arena of MAVs<sup>7</sup>. For a good overview of the effect of Reynolds number and aspect ratio on small wings, see Ol *et al.*<sup>8,9</sup>

Most models used for flight control rely on the quasi-steady assumption that lift and drag forces depend on parameters such as relative velocity and angle of attack in a static manner. While these models work well for conventional aircraft<sup>10</sup>, they do not describe the unsteady laminar separation characteristics of flows over small, agile wings, for which the dynamics, or time history, of these parameters become important. There are a number of classical theories for unsteady airfoil motion which have been used to study flutter induced instabilities<sup>11,12</sup> and to predict the response of an airfoil to a given maneuver in time<sup>13,14</sup>. Despite the wide variety of extensions and uses for these theories<sup>15</sup>, they rely on a number of limiting idealizations, such as infinitesimal motions in an inviscid fluid, which exclude the important cases where flow is separated.

In order to develop controls suitable for unsteady aerodynamics, it is essential to have a framework of models which are both physically accurate and computationally tractable. Low order ODE models for unsteady forces are ideal for control design because they fit naturally into existing flight dynamics models. However, during rapid flight

\*Graduate Student, Mechanical and Aerospace Engineering, Student Member.

†Associate Professor, Mechanical and Aerospace Engineering, Senior Member.

maneuvers for which traditional models are invalid, the governing flow equations are significantly complicated by the unsteadiness of the Navier-Stokes equations<sup>16</sup>. Reduction of the governing PDE to a low dimensional set of ODE models has been the subject of much theoretical effort<sup>17</sup>. Computational fluid dynamics offers a number of advantages for model reduction. New techniques developed for simulation<sup>18,19</sup> and visualization<sup>20,21</sup> of complex flows allow us to investigate the physical mechanisms underlying the dynamics of laminar separation. In addition to body force data which is less noisy than wind tunnel measurements, direct simulation results in full velocity fields at a number of time snapshots. With velocity field snapshots, it is possible to obtain reduced order models by projective methods such as balanced truncation or proper orthogonal decomposition<sup>22</sup> (POD). In contrast, a bottom-up approach involving simple nonlinear models which are phenomenologically motivated<sup>23,24</sup> may lead to more natural control design. Here, we pursue both approaches to obtain reduced order models.

This paper is organized as follows: in Section II, we introduce the computational methods used to simulate and visualize flow experiments. Section III demonstrates the use of POD modes and Galerkin projection to obtain reduced order models for the periodic laminar vortex shedding over a flat plate in Reynolds number 100 flow for fixed angles of attack  $\alpha = 30^\circ$  and  $\alpha = 45^\circ$ . Section IV compares classical unsteady aerodynamic models, such as Theodorsen's and Wagner's indicial response, with DNS for pitching and plunging airfoils over a range of parameter conditions; special attention is given to identifying when traditional models break down. Finally, we conclude with a discussion of results and some interesting future directions.

## II. Simulation & Visualization

### A. Immersed boundary method

The work that follows relies on fully resolved direct numerical simulations (DNS) performed using an immersed boundary method developed at Caltech<sup>18,19,25-27</sup>. With this code, it is possible to construct incompressible flow experiments at low Reynolds numbers ( $< 1000$ ) and obtain velocity snapshots of the flow field. The method efficiently solves the incompressible Navier-Stokes equations using a fractional step method on a set of nested grids centered around the movable body. Typically five grids, each having the same number of grid points (at least  $200 \times 200$ ), are nested so that the finest grid is defined on a spatial domain of  $4 \times 4$  (nondimensionalized by chord) and the coarsest grid is defined on a domain  $64 \times 64$ . A convergence study was performed at  $Re = 300$  for a stationary plate with  $\alpha = 45^\circ$ , and grid independence was achieved at this configuration.

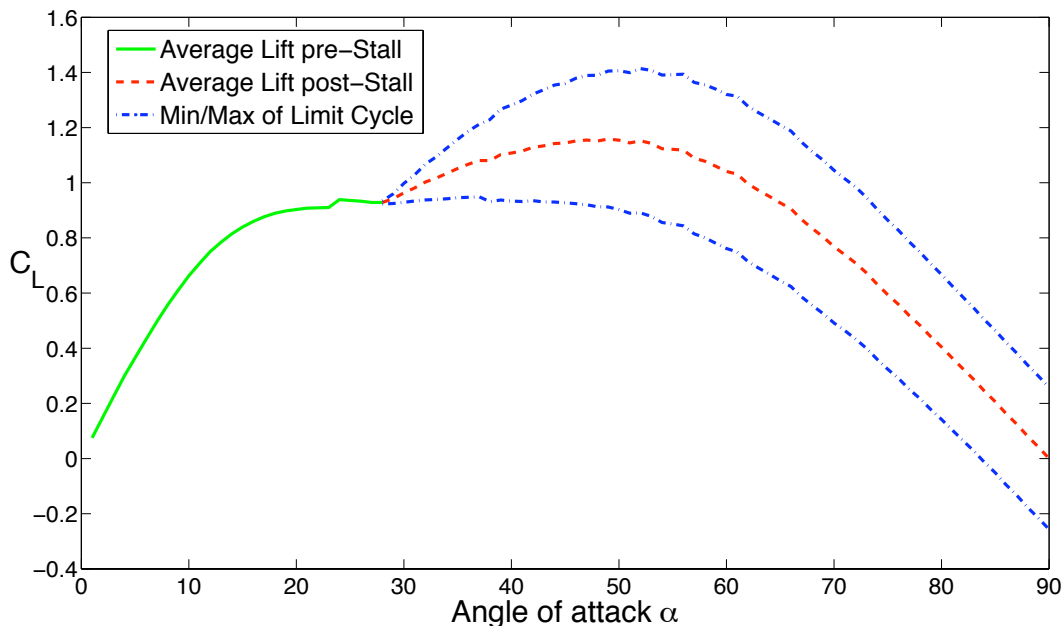


**Figure 1.** Lift coefficient vs. angle of attack for fixed plate at  $Re = 100$ . A supercritical Hopf bifurcation occurs at  $\alpha \approx 28^\circ$ . The dashed line represents average post-stall lift and the dotted lines represent minimum and maximum post-stall lift.

Here, we describe the results of 2D simulations performed at a Reynolds number range of 100-300 on the multiple grid configuration discussed above; the finest-scale grid is defined on a  $4 \times 4$  domain, the coarsest grid is defined on a  $64 \times 64$  domain, and the number of points in each grid is at least  $200 \times 200$ . In previous studies<sup>24</sup>, the steady-state lift of a flat plate was computed for angle of attack  $\alpha \in [0, 90]$ , exhibiting a bifurcation in lift at  $\alpha_c \approx 28^\circ$ , as seen in Figure 1. For  $\alpha > \alpha_c$ , a stable limit cycle develops, corresponding to periodic vortex shedding from the leading and trailing edge. Using an eigenvalue analysis and solving for the unstable equilibrium which appears for  $\alpha > \alpha_c$  by Newton-Krylov iterations, it has been verified that the flow undergoes a Hopf bifurcation<sup>7</sup>.

## B. Lagrangian coherent structures

To characterize the unsteady fluid dynamics of airfoils at low Reynolds numbers, it is important to identify regions of separated flow as well as wake structures. For an unsteady flow field, it is not possible to identify separated regions with streamlines alone<sup>20</sup>. Lagrangian coherent structures<sup>17,21,28,29</sup> (LCS), which are computed from a time-resolved sequence of snapshots of an unsteady flow, indicate regions of large stretching between nearby particles as ridges in the field of finite time Lyapunov exponents (FTLE) that satisfy an additional hyperbolicity condition<sup>20</sup>. FTLE fields may be computed using backward (resp. forward) time integration of particle grids, in which case the LCS represents attracting (resp. repelling) material lines and isolate regions of separated flow around the plate and sluggish flow in the wake. In the following visualizations, FTLE fields measuring stretching in backward time are used to obtain structures that attract particles in forward time. FTLE fields for four interesting cases are shown in Figure 2, where ridges, plotted in blue, indicate the boundaries of a separation bubble. For the case of a stationary plate at  $\alpha = 25^\circ$ , the ridges coincide with streamlines outlining the separation bubble, since the flow field is steady; however, for each of the other three unsteady cases, the FTLE ridges are not the same as streamlines.

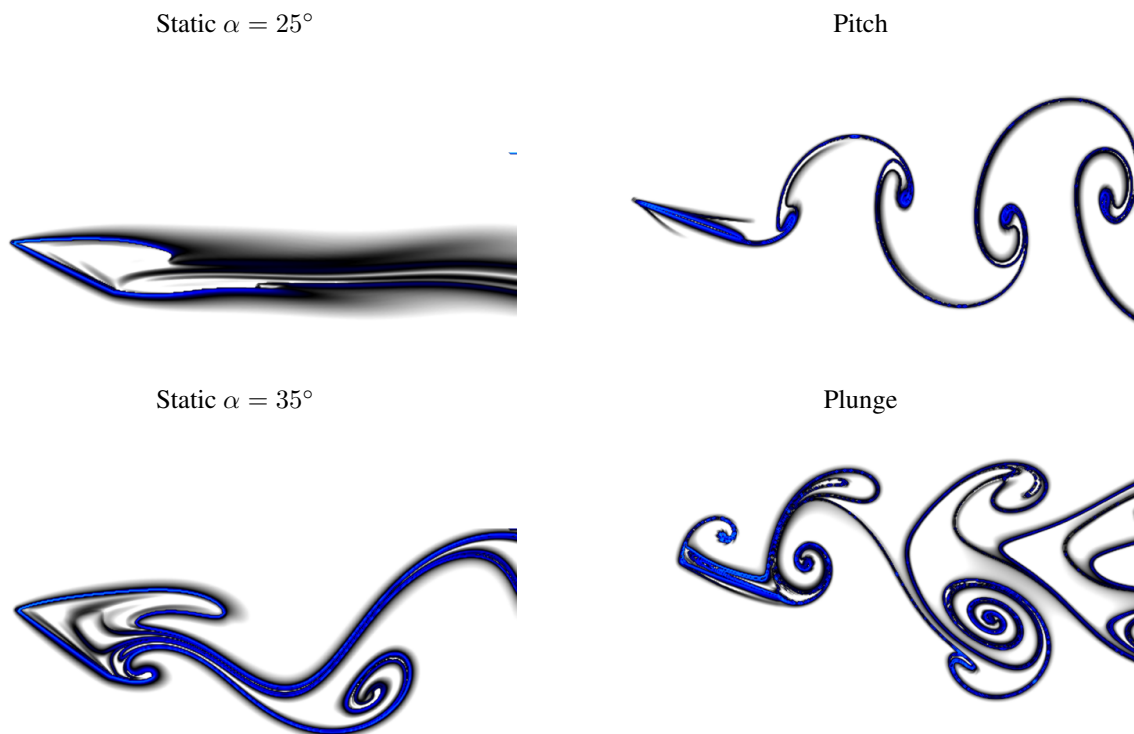


**Figure 2.** Lagrangian coherent structures for a variety of stationary and moving plates. (Top Left) Stationary plate at  $\alpha = 25^\circ$  (Bottom Left) Stationary plate at  $\alpha = 35^\circ$  (Top Right) Pitching plate (Bottom Right) Plunging plate with  $20^\circ$  bias. Ridges in the FTLE field are plotted in blue and represent the boundaries of a separation bubble. The flow field associated with a stationary plate at  $\alpha = 25^\circ$  is the only steady case, and in thus FTLE ridges coincide with streamlines. In each of the other cases, FTLE ridges do not coincide with streamlines.

To compute the FTLE field at a given moment in time, the first step is to initialize a grid of particles across the spatial domain of interest and advect (integrate) these particles either forward or backward in time using velocity field snapshots from DNS or PIV. Choice of integration time,  $T$ , is important since this will determine the number of structures the particles interact with. Finite differencing of particle positions after integration with respect to their initial positions provides a discrete approximation to the Cauchy-Green deformation tensor  $\Delta$ . The eigenvalues of  $\Delta$  indicate magnitudes of particle stretching along principal directions; the largest eigenvalue is directly related to the

finite time Lyapunov exponent:

$$\sigma_T(x) = \frac{1}{|T|} \log \sqrt{\lambda_{\max}(\Delta)} \quad \Delta = \frac{d\varphi_T}{dx}^* \frac{d\varphi_T}{dx}$$

Although straightforward, this method is computationally intensive and involves a number of redundant particle integrations for neighboring FTLE fields in time. A fast method for FTLE computation<sup>30</sup> has recently been developed to speed up time-series of FTLE calculations.

### III. Proper orthogonal decomposition & Galerkin projection

The evolution of a flow field via direct numerical simulation may be viewed as a high dimensional dynamical system  $\dot{u} = X(u)$ , where  $u$  is a state variable representing the velocity components at each spatial location, arranged in a long vector. Therefore,  $u \in \mathbb{R}^N$  where  $N$  is the number of grid points times the number of flow variables. Although modern desktop and cluster computing have made direct numerical simulations possible for increasingly large problems, the full discretized dynamics are still intractable for real-time predictive control. Moreover, it is not feasible to apply powerful tools from dynamical systems theory, such as normal form expansions and bifurcation analysis, to systems of such large dimension. Instead, it is desirable to obtain reduced order models, or ODEs of dimension  $n \ll N$ , which agree well with the full dynamics. In addition to their utility in real-time control applications, these simplified models provide a starting point for understanding the bifurcation structure of the full system and how various parameters enter into the dynamics.

To obtain a reduced order model, it is first necessary to construct a low dimensional subspace  $S \subset \mathbb{R}^N$  on which the dynamics may be projected. Given a time sequence of unsteady velocity fields  $\{u_k \in \mathbb{R}^N\}_{k=1}^M$  from DNS, we seek a projection  $P_S : \mathbb{R}^N \rightarrow S$  so that the projection error  $\frac{1}{M} \sum_{k=1}^M (\|u_k - P_S u_k\|)$  is minimized. It has been shown that this minimization problem is equivalent to the eigenvalue problem

$$R\varphi = \lambda\varphi \quad \text{where} \quad R = XX^* \quad \text{and} \quad X = \begin{bmatrix} \vdots & \vdots & & \vdots \\ u_1 & u_2 & \dots & u_M \\ \vdots & \vdots & & \vdots \end{bmatrix}$$

$R$  is a real, symmetric matrix of dimension  $N \times N$  with at most  $M$  nonzero eigenvalues. Therefore, the eigenvalue problem  $R\varphi = \lambda\varphi$  is equivalent to a simpler eigenvalue problem

$$U\varphi = \lambda\varphi \quad \text{where} \quad U = X^*X$$

of dimension  $M \times M$ . For  $M \ll N$ , this greatly reduces the computation and is known as the method of snapshots.  $\{\varphi_k\}_{k=1}^m$  are eigenfunctions associated with the  $m$  largest eigenvalues of  $R$  (or  $U$ ) and are known as POD modes. POD modes are typically computed after subtracting the mean flow from each of the snapshots  $u_i$ . Because of the form of the minimization problem posed, the first  $k$  POD modes are the  $k$  most energy-containing modes. Although energetic modes are important, it has been shown that modes including only a small fraction of the total energy can be dynamically important<sup>31</sup>.

Given dynamics  $\dot{u} = X(u)$  and a projection  $P_S$  onto a low dimensional subspace  $S \subset \mathbb{R}^N$ , it is now possible to project the discretized Navier-Stokes equations onto the subspace  $S$ , resulting in a low order dynamical system model for the full equations of motion:

$$\dot{r} = P_S X(r), \quad \text{where} \quad r(t) = \bar{\varphi} + \sum_{k=1}^m a_k(t) \varphi_k$$

The dynamics are now captured as a low dimensional ODE with the POD mode amplitudes as variables:

$$\begin{aligned} \langle \dot{r} - X(r), \varphi_k \rangle = 0 &\implies \langle \dot{a}_j \varphi_j, \varphi_k \rangle - \langle X(r), \varphi_k \rangle = 0 \\ &\implies \dot{a}_k = \langle X(r), \varphi_k \rangle \quad \text{for} \quad k = 1, \dots, m \end{aligned}$$

In the current study,  $\dot{u} = X(u)$  is the momentum equation:

$$\dot{u} = \underbrace{-(u \cdot \nabla)u + \nu \nabla^2 u - \nabla p}_{X(u)}$$

Although Galerkin projection is an important method of obtaining a dynamical systems related to the DNS, it is possible to use the variables of a phenomenological ODE model as amplitudes of POD modes.

### A. POD/Galerkin model - $Re = 100$ , $\alpha = 45^\circ$

From simulation data of unsteady flow around a fixed plate at  $Re = 100$  and  $\alpha = 45^\circ$  which are allowed to reach steady state vortex shedding, POD modes are computed and shown in Figure 4. In this configuration the plate sheds vorticity periodically from the leading and trailing edges. By first subtracting the mean flow, it is possible to obtain POD modes which are in energetic pairs as seen in the eigenvalue plot, Figure 3. Because of an approximate convective symmetry in the periodic shedding case, these POD modes come in pairs which appear to be phase shifted by  $\pi/2$ .

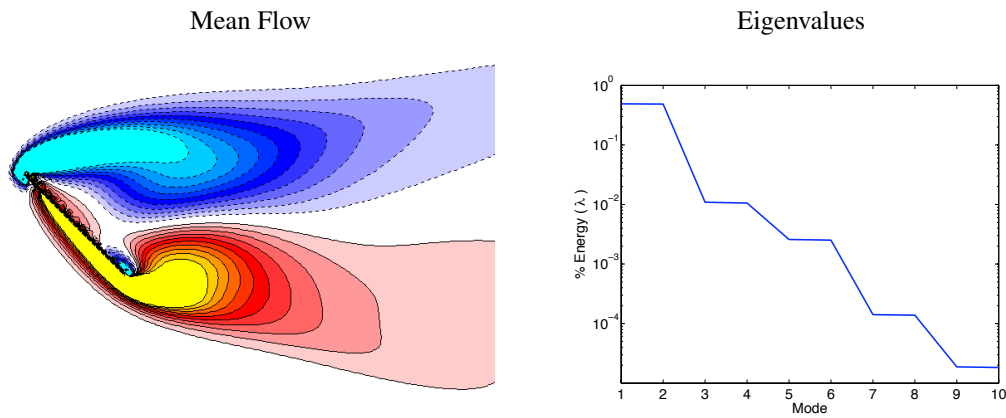


Figure 3. Mean flow and eigenvalues of POD modes for stationary flat plate at  $\alpha = 45^\circ$  and  $Re = 100$ .

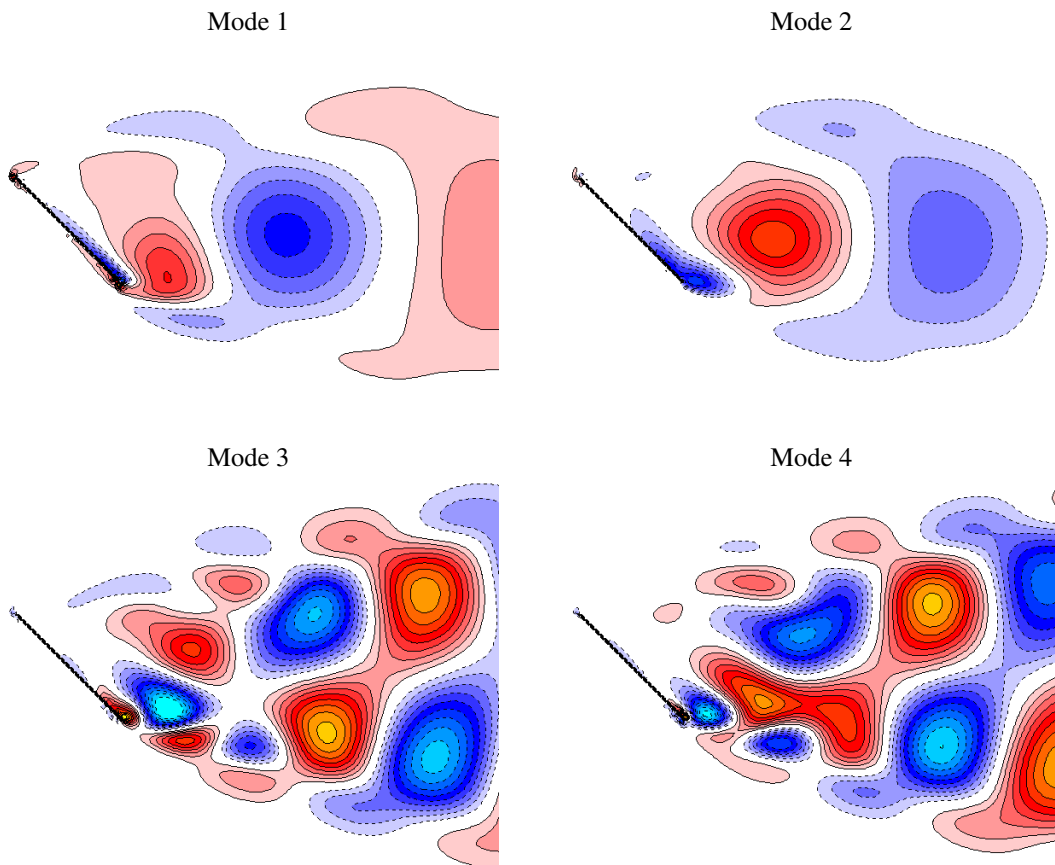


Figure 4. POD modes for stationary flat plate at  $\alpha = 45^\circ$  and  $Re = 100$ .

## B. POD/Galerkin model - $Re = 100$ , $\alpha = 30^\circ$

Figure 6 shows POD modes for the unsteady flow around a fixed plate at  $Re = 100$  and  $\alpha = 30^\circ$ . The eigenvalue plot, Figure 5, is similar to the  $\alpha = 45^\circ$  case, except that the pairs are not as closely matched.

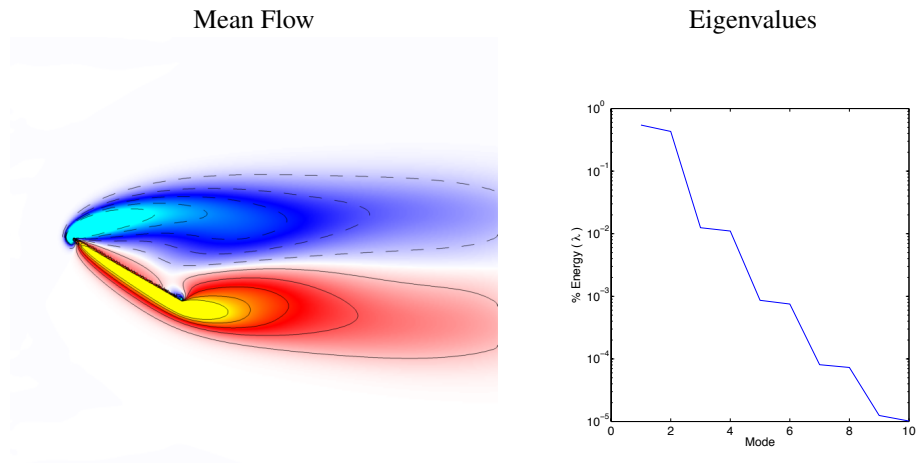


Figure 5. Mean flow and eigenvalues of POD modes for stationary flat plate at  $\alpha = 30^\circ$  and  $Re = 100$ .

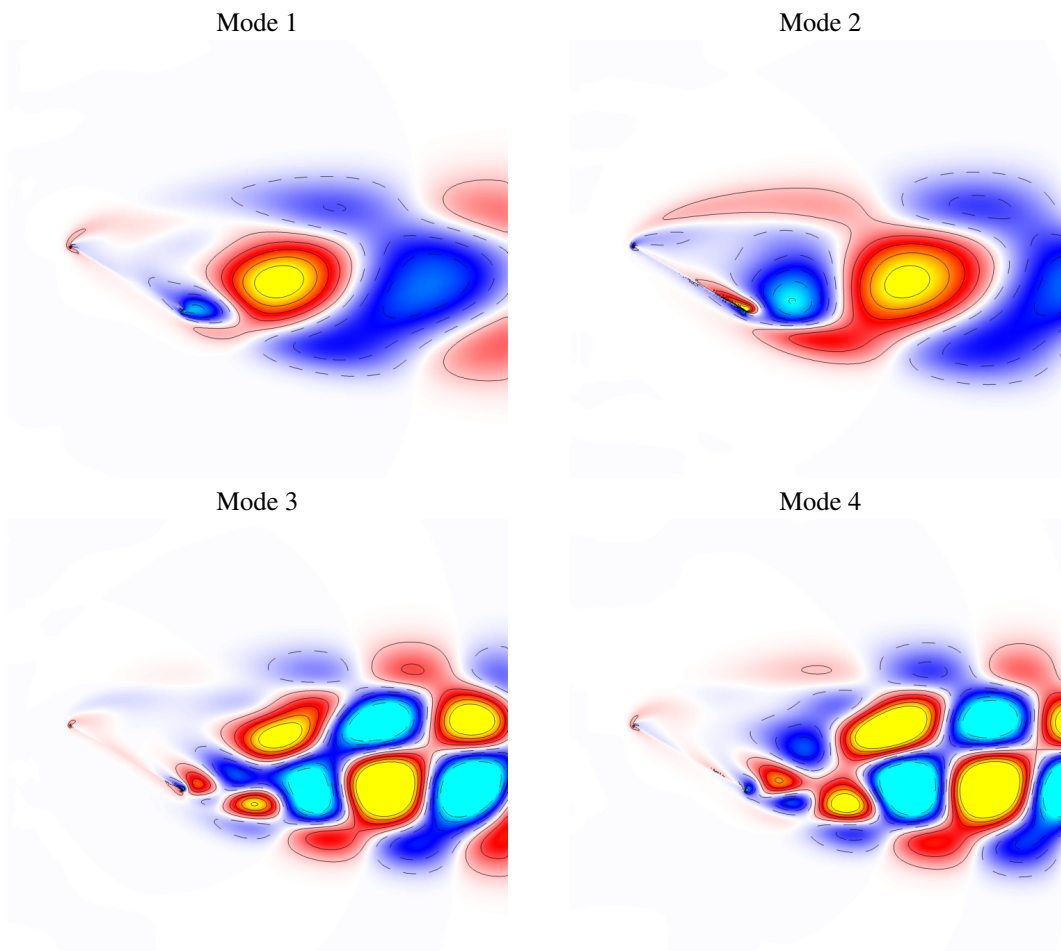


Figure 6. POD modes for stationary flat plate at  $\alpha = 30^\circ$  and  $Re = 100$ .

A low order model is obtained by Galerkin projecting the Navier-Stokes equations onto these modes. Using the projected dynamics, the POD mode coefficients are integrated forward in time and used to reconstruct an approximate flow field. From the approximate velocity field reconstruction, an FTLE field is computed which agrees very well

with the FTLE field from DNS, as can be seen in Figure 7. The comparison of POD mode amplitudes between DNS and projected dynamics is shown in Figure 8. It is interesting that the model agrees well with data for the first two modes, but not for the higher order modes. However, the fact that the Lagrangian coherent structures are preserved suggests that the first two modes are sufficient for reconstructing an accurate model. This is not entirely surprising considering the very simple sinusoidal vortex shedding pattern and force in time. For higher Reynolds number flows, the lift distribution and wake structures involve higher frequency oscillations which would presumably require more modes to approximate.

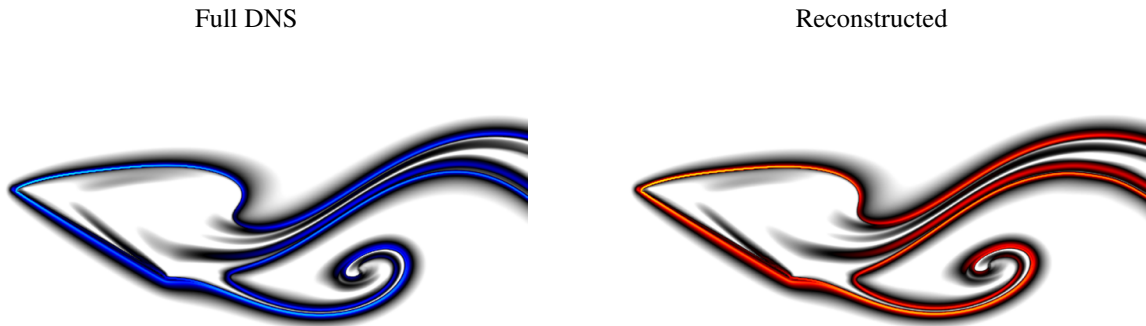


Figure 7. FTLE field for DNS vs. reconstruction from Galerkin projected dynamics for stationary flat plate at  $\alpha = 30^\circ$  and  $Re = 100$ .

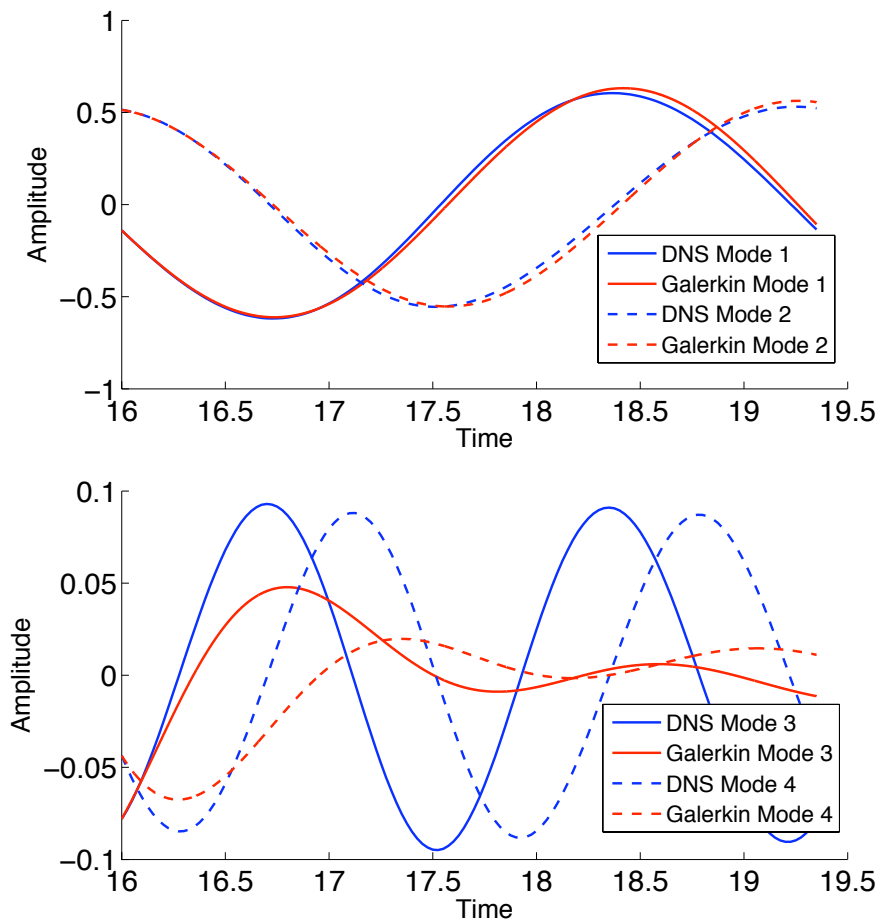


Figure 8. Mode amplitudes of DNS vs. reconstruction from Galerkin projected dynamics for stationary flat plate at  $\alpha = 30^\circ$  and  $Re = 100$ .

## IV. Classical unsteady aerodynamic models

When modeling the aerodynamic forces acting on an airfoil in motion, it is natural to start with a quasi-steady approximation. Instead of dealing with the full unsteady problem, one assumes that the airfoil's center of mass,  $h$ , and angle of attack,  $\alpha$ , motions are "gradual" enough for the flow field to locally equilibrate to the motion. In this way, the unsteady terms in the flow equations are set to zero and the motion is accounted for by translating  $\dot{h}$  into an effective angle of attack and  $\dot{\alpha}$  into an effective camber. Finally, applying the assumption of a thin airfoil, we obtain a quasi-steady estimate for the lift coefficient

$$C_L = 2\pi \left( \alpha + \dot{h} + \frac{1}{2}\dot{\alpha} \left( \frac{1}{2} - a \right) \right) \quad (1)$$

Lengths are nondimensionalized by  $2b$  and time is nondimensionalized by  $2b/U_\infty$ , where  $U_\infty$  is the free stream velocity,  $b$  is the half-chord length and  $a$  is the pitch axis location with respect to the 1/2-chord (e.g., pitching about the leading edge corresponds to  $a = -1$ , whereas the trailing edge is  $a = 1$ ).

In 1935, Theodorsen<sup>11</sup> went beyond the quasi-steady models and solved for the lift distribution around an idealized airfoil in purely sinusoidal pitch and plunge maneuvers. His theory is soluble with analytic techniques, relying on a number of simplifications, such as an inviscid, incompressible flow field and infinitesimal deflections of a flat plate, leaving an idealized planar wake. Because his theory was developed to handle purely sinusoidal maneuvers, it is represented in the frequency domain. Theodorsen's model predicts the unsteady lift as

$$C_L = \underbrace{\frac{\pi}{2} \left[ \ddot{h} + \dot{\alpha} - \frac{a}{2}\ddot{\alpha} \right]}_{\text{Apparent Mass}} + \underbrace{2\pi \left[ \alpha + \dot{h} + \frac{1}{2}\dot{\alpha} \left( \frac{1}{2} - a \right) \right]}_{\text{Circulatory}} C(k)$$

where Theodorsen's function  $C(k)$  is a transfer function relating sinusoidal inputs of reduced frequency<sup>32</sup>  $k$  to their aerodynamic response. The first set of terms represent the "apparent mass", or non-circulatory terms. The second set of terms are due to circulatory effects, and are exactly the quasi-steady forces multiplied by Theodorsen's function, which accounts for the change in magnitude and phase of these terms with changes in reduced frequency. This expression simplifies considerably for an airfoil in pure pitch or pure plunge

$$\text{pure plunge } (\alpha = 0) \quad C_L = \frac{\pi}{2}\ddot{h} + 2\pi\dot{h}C(k) \quad (2)$$

$$\text{pure pitch} \quad C_L = \frac{\pi}{2} \left[ \dot{\alpha} - \frac{a}{2}\ddot{\alpha} \right] + 2\pi \left[ \alpha + \frac{1}{2}\dot{\alpha} \left( \frac{1}{2} - a \right) \right] C(k) \quad (3)$$

In 1925, Wagner<sup>13</sup> developed a time domain theory for the similar problem of an idealized airfoil undergoing motion of an arbitrary time history. The idea is simple: given a transient and steady state lift  $C_L^\delta(t)$  due to a step response in angle-of-attack,  $\dot{\alpha} = \delta(t)$ , it is possible to reconstruct the lift response to arbitrary  $\alpha(t)$  using Duhamel superposition.

$$C_L^{\alpha(t)}(t) = C_L^\delta(t)\alpha(0) + \int_0^t C_L^\delta(t - \tau)\dot{\alpha}(\tau)d\tau \quad (4)$$

There are a number of interesting generalizations to these methods, such as the methods of Sears<sup>33</sup> and Küssner<sup>14</sup> which extended the methods of Theodorsen and Wagner, respectively, to the problem of moving wind direction, rather than moving airfoil. However, this section is meant to provide a brief review of the classical tools developed for modeling unsteady aerodynamic forces in the 1920s-1950s. A more complete treatment of the subject can be found in Leishman<sup>15</sup>.

### A. Theodorsen's Model - Sinusoidally Plunging Airfoil

Using equations (1) and (2) it is possible to compare the thin airfoil theory and Theodorsen's model with the simulated response of a flat plate to sinusoidal plunging in Reynolds number 100 flow. It is also compared with an *effective* angle of attack approximation by using a look up table for the lift coefficient at the static angle of attack  $\alpha_{\text{eff}}(t) = \tan^{-1}(-\dot{h}(t)/U_\infty)$  for each point in the maneuver; this approximation may be classified as quasi-steady. The plunging motion is specified by the center of mass motion  $h(t) = -A \sin(\omega t)$ .

It was previously shown<sup>24</sup> that for reasonable Strouhal numbers and reduced frequencies  $k = \pi fc/U_\infty$  less than 0.5, the effective angle of attack approximation agrees well with DNS. However, for the same range of Strouhal numbers  $St \in \{.032, .064, .128\}$ , we find that Theodorsen's theory agrees with DNS up to reduced frequencies of 2.0,

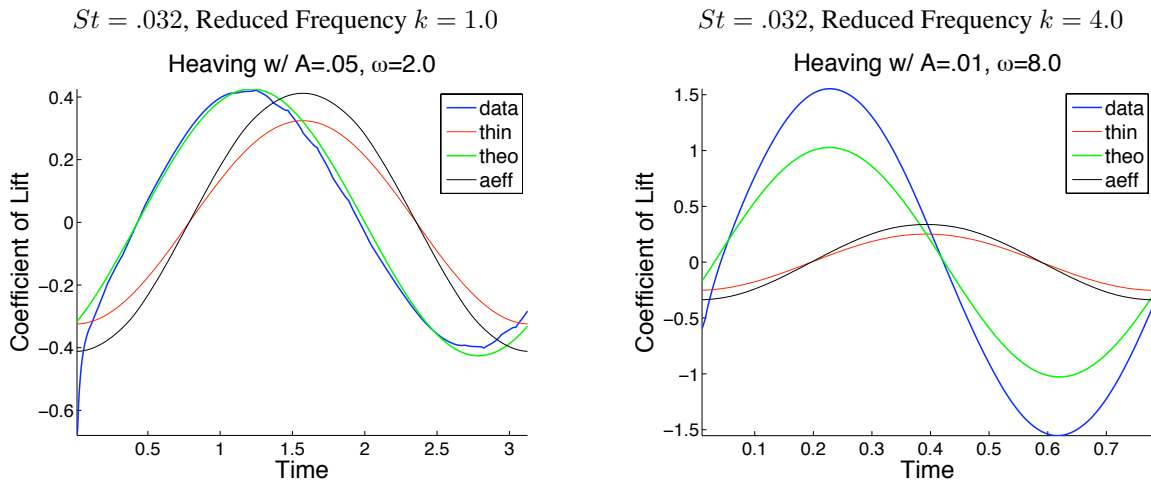


Figure 9. Each curve is a plot of lift coefficient vs. time for a sinusoidally plunging flat plate at  $Re = 100$  and Strouhal number  $.032$ . The blue curve is the  $C_L$  from DNS, the red curve is computed using thin airfoil theory, Eq. (1), the black curve uses an effective angle of attack approximation, and the green curve is Theodorsen’s prediction, Eq. (2). Theodorsen’s model agrees well with DNS for reduced frequencies  $k < 2.0$  as long as the Strouhal number is small enough that the maximum effective angle of attack is less than the stall angle.

shown in Figure 9. This is consistent, since at larger reduced frequencies, quasi-steady assumptions break down and it becomes important to consider flow acceleration terms.

For larger Strouhal numbers,  $St \in \{.256, .512\}$ , Theodorsen’s model disagrees with DNS even for small reduced frequencies, shown in Figure 10. This is particularly interesting, because these large Strouhal numbers correspond to maximum effective angles of attack which are larger than the critical stall angle shown in Figure 1. At these Strouhal numbers the effective angle of attack approximation plateaus due to  $\alpha_{eff} > \alpha_c$ . In addition to disagreeing with DNS in magnitude and phase, Theodorsen’s model does not describe the higher-frequency components in the response.

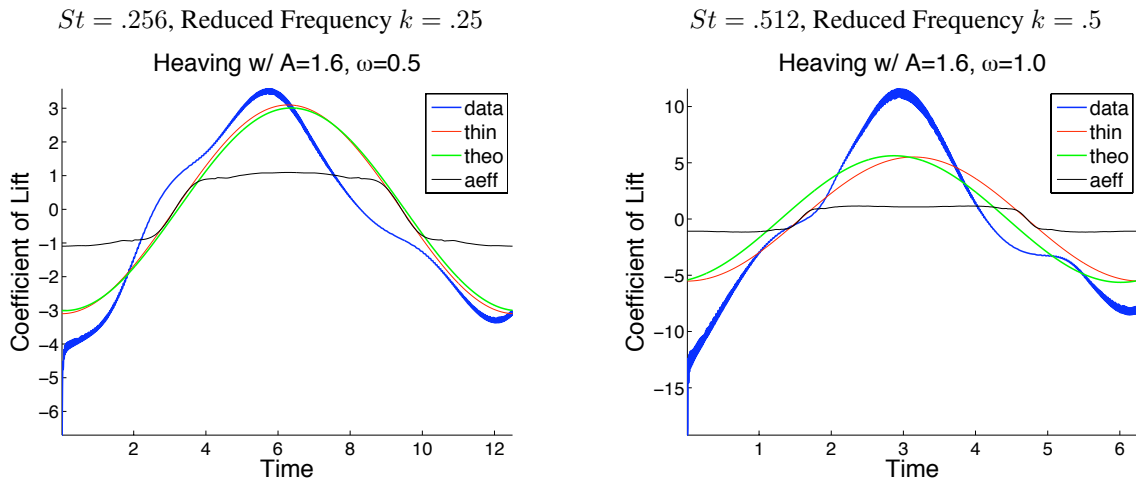


Figure 10. Each curve is a plot of lift coefficient vs. time for a sinusoidally plunging flat plate at  $Re = 100$  and Strouhal numbers  $.256$  and  $.512$ . The blue curve is the  $C_L$  from DNS, the red curve is computed using thin airfoil theory, Eq. (1), the black curve uses an effective angle of attack approximation, and the green curve is Theodorsen’s prediction, Eq. (2). For large Strouhal numbers, Theodorsen’s model does not agree well with DNS even at low reduced frequency. Also, there are higher frequency components which are not captured by the models.

The table below shows the maximum effective angle of attack associated with each Strouhal number used above. Notice that for Strouhal numbers  $.256$  and  $.512$ , the maximum effective angle of attack is larger than the critical stall angle  $\alpha_c \approx 28^\circ$ .

Strouhal number ( $St$ )	.032	.064	.128	.256	.512
Max effective aoa ( $\alpha_{eff}^{max}$ )	$5.74^\circ$	$11.37^\circ$	$21.91^\circ$	$38.81^\circ$	$58.13^\circ$

## B. Theodorsen's Model - Sinusoidally Pitching Airfoil

Similar to the case of a sinusoidally plunging airfoil, with equation (3) it is possible to compare Theodorsen's model with DNS for a sinusoidally pitching flat plate. Three pitching amplitudes  $\alpha \in \{20^\circ, 27.1^\circ, 43.2^\circ\}$  are examined, and for each amplitude the pitching point is varied along the chord from the leading-edge to the trailing-edge at every quarter-chord in between. In each case, the reduced frequency is  $k = 1.26$ . Interestingly, the agreement between Theodorsen's model and DNS does not depend so much on reduced frequency and Strouhal number as in the case of sinusoidal plunging, but instead depends much more on raw pitching amplitudes and pitching point. In Figure 11 we see that for the same angle of attack excursion Theodorsen's model agrees better with DNS when the plate pitches about the leading edge, even though the Strouhal number is larger.

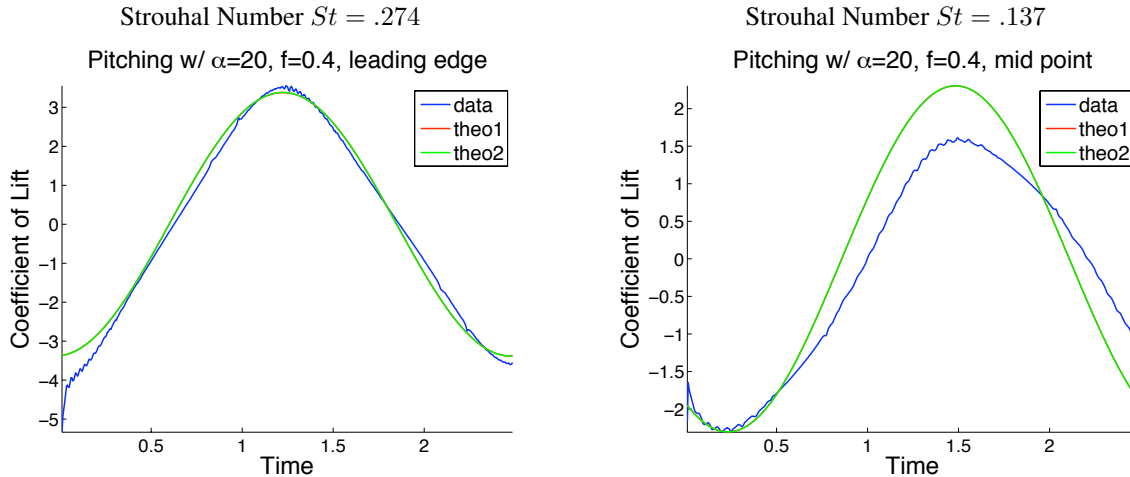


Figure 11. Each curve is a plot of lift coefficient vs. time for a sinusoidally pitching flat plate at  $Re = 100$  and reduced frequency  $k = 1.26$ . The blue curve is the  $C_L$  from DNS, and the green curve is Theodorsen's prediction, Eq. (3). Theodorsen's model matches DNS for a flat plate pitching to an amplitude of  $20^\circ$  about the leading edge and not the half-chord, even though the Strouhal number is larger for pitching about the leading edge.

This is consistent with the fact that Theodorsen's theory depends on the assumption of attached flow over the wing surface, and pitching about the mid-chord promotes leading-edge separation much more than pitching about the leading edge. This effect is shown in Figure 12, where the effect of leading edge separation is exaggerated due to the large pitch amplitude  $\alpha_{max} = 27.1^\circ$ .

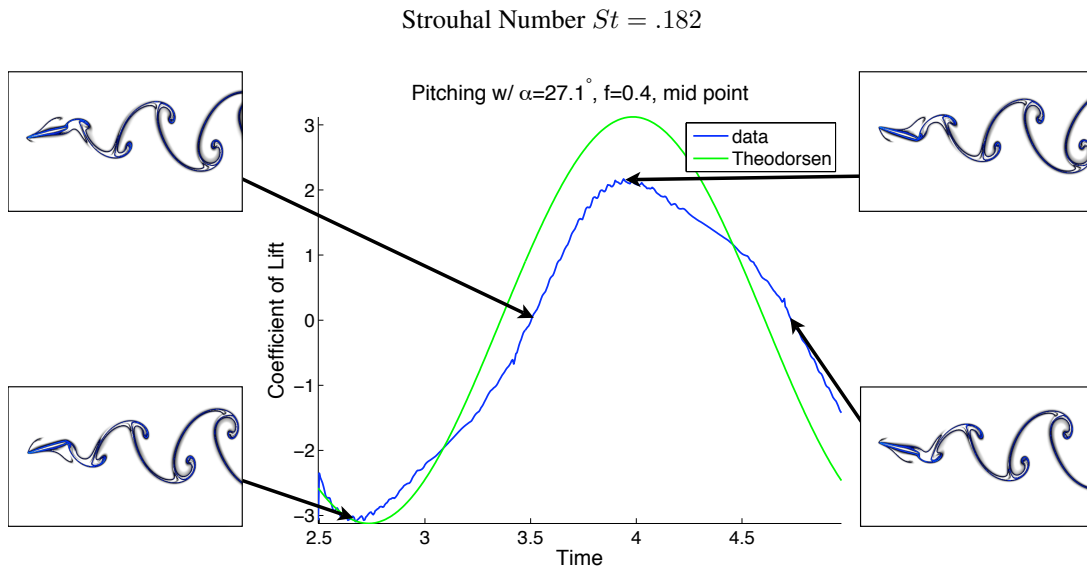


Figure 12. Leading edge separation is visualized using FTLE fields for a plate pitching to an amplitude of  $27.1^\circ$  about the mid chord.

When the pitch amplitude is larger than the stall angle  $\alpha_c \approx 28^\circ$ , Theodorsen's model does not agree with DNS even when the plate is pitched about the leading edge; see Figure 13. This is interesting because there is a similar observation in the case of sinusoidal plunging, where Theodorsen's model begins to disagree at Strouhal numbers which correspond to effective angles of attack larger than  $\alpha_c$ . This should not be surprising, however, since Theodorsen's theory is developed for infinitesimal oscillations where the flow is never separated and the wake is assumed to be planar. Under these assumptions, Theodorsen's model cannot possibly take high angle of attack vortex shedding effects into account.

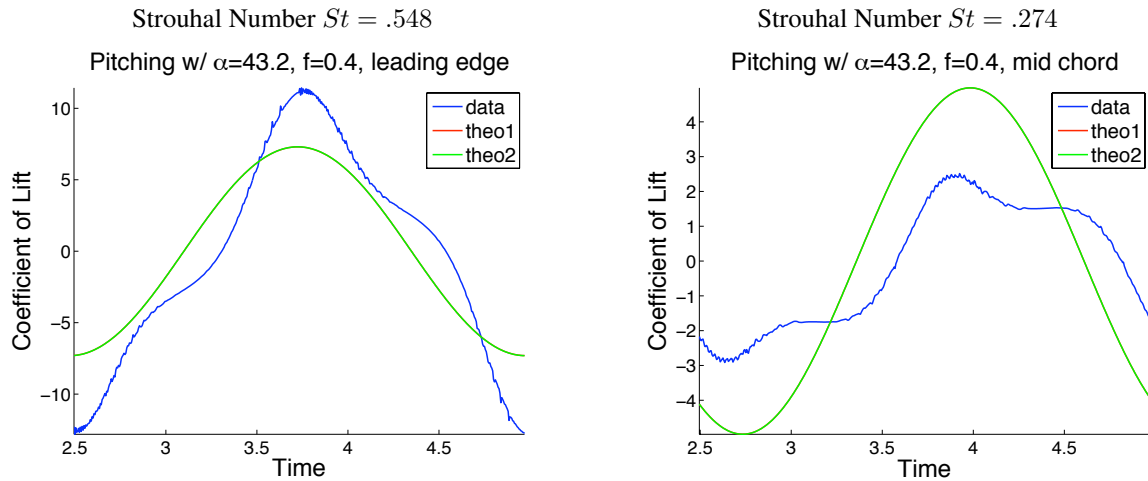


Figure 13. Each curve is a plot of lift coefficient vs. time for a sinusoidally pitching flat plate at  $Re = 100$  and reduced frequency  $k = 1.26$ . The blue curve is the  $C_L$  from DNS, and the green curve is Theodorsen's prediction, Eq. (3). For pitching amplitude  $\alpha_{max} = 43.2^\circ > \alpha_c$ , Theodorsen's model doesn't agree with DNS, despite the pitching point.

In addition to the lack of agreement between Theodorsen's model and DNS for large pitching amplitudes, there are  $C_L$  variations at twice the pitching frequency, as there was in the case of sinusoidal plunging for Strouhal numbers  $St \in \{.256, .512\}$ . Using FTLE to visualize the flow structures, it is possible to see not only leading edge separation, but also a distortion of the FTLE near the plate near the mid chord, as shown in Figure 14. It is likely that natural vortex shedding at this high angle of attack is interacting with the separation due to the airfoils pitching motion.

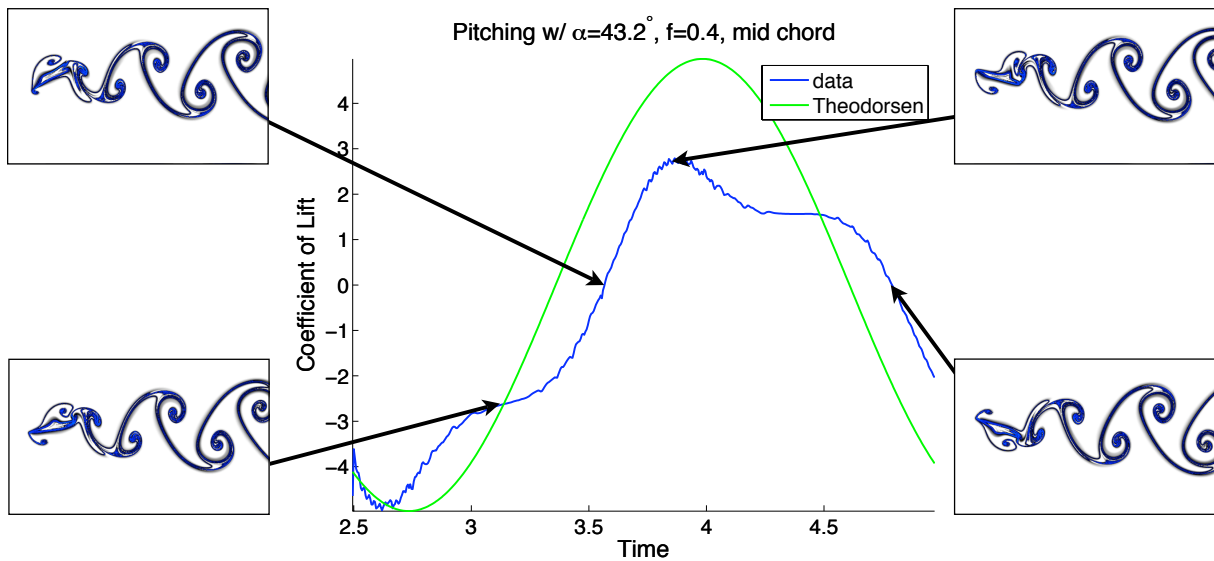
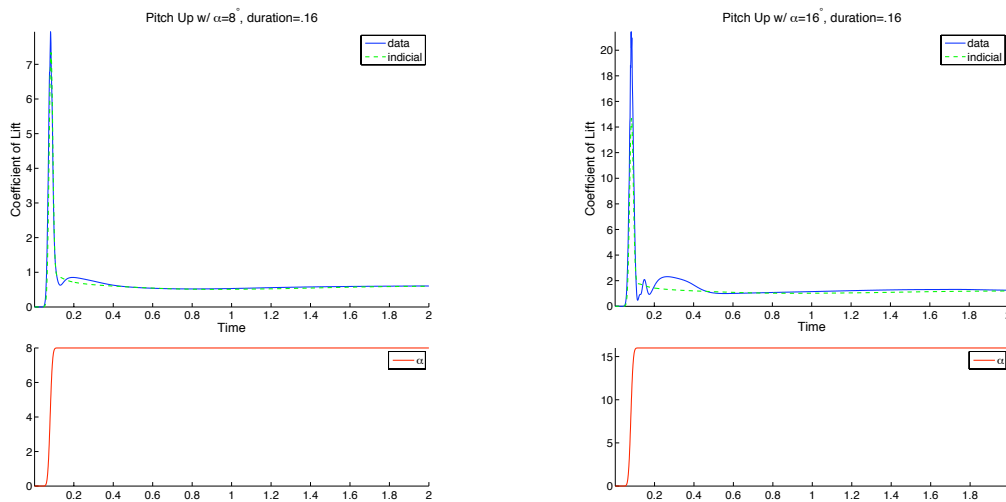


Figure 14. Leading edge separation is visualized using FTLE fields for a plate pitching to an amplitude of  $43.2^\circ$  about the mid chord.

### C. Indicial Response

Compared with Theodorsen’s method of predicting response forces, indicial response, equation (4) is an empirical method which relies on knowing only the response in lift to a small step in angle of attack. For the simulations below, the step in  $\alpha$  was approximated by a steep sigmoidal step of  $1^\circ$ . The indicial response roughly predicts the initial peak observed in DNS for fast pitch-up maneuvers of moderate amplitude,  $\alpha = 8^\circ$  and  $\alpha = 16^\circ$ , shown in Figure 15. However, superposition of a number of small steps fails to reproduce transient oscillations as the initial peak dies off.



**Figure 15. (top) Comparison of lift coefficient,  $C_L$ , between DNS and Indicial response for a flat plate in pitch-up maneuver at  $Re = 300$ . (bottom) Angle of attack vs. time. (left) Pitch-up of  $8^\circ$  with duration of 16 time steps. (right) Pitch-up of  $16^\circ$  with duration 16 time steps**

For larger angle of attack pitch-up maneuvers, say  $\alpha = 32^\circ$ , the indicial response predicts the rough form of transient lift, but doesn’t capture the jagged peak which is observed in DNS. Because the method of indicial response involves staggered superposition of a number of small steps to reconstruct a large step, it is not possible for this method to predict the periodic vortex shedding which is characteristic of high angles of attack. Therefore, even if it is able to predict transient lifts, it is not useful for steady state prediction at large angle of attack, as shown in Figure 16.

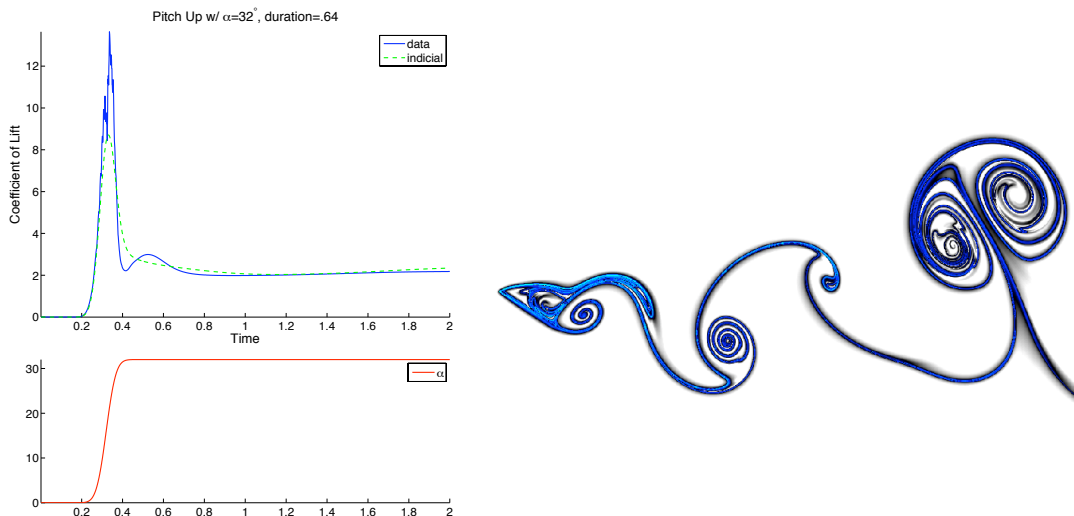


**Figure 16. (left) Comparison of lift coefficient,  $C_L$ , between DNS and Indicial response for a flat plate in pitch-up at  $Re = 300$  and sinusoidal pitch maneuver at  $Re = 100$ . (right) FTLE field visualization of the periodic laminar vortex shedding which takes place after the transients die down.**

## V. Conclusions and Future Directions

We have investigated the unsteady aerodynamic forces on low-Reynolds number wings at high angle of attack and in pitch and plunge maneuvers using 2D direct numerical simulations. The classical theories of Theodorsen and Wagner have been compared with DNS for a number of pitch and plunge maneuvers of varying Strouhal number, reduced frequency, pitch amplitude and center. In addition to determining when these theories break down, the flow field is investigated using FTLE to visualize relevant flow structures to determine *how* the theories break down, indicating possible improvements to the models. Velocity field snapshots from DNS are used to extract POD modes for flow over a flat plate at high angle of attack for Reynolds number 100. The Navier-Stokes equations are then projected onto these modes resulting in a low order model which captures the periodic vortex shedding and preserves Lagrangian coherent structures.

Comparison of Theodorsen's model for the lift of a sinusoidally plunging flat plate with forces from DNS showed agreement for moderate reduced frequencies  $k < 2.0$  for a range of Strouhal numbers for which the maximum effective angle of attack is smaller than the critical stall angle. For the case of a sinusoidally pitching plate, agreement between Theodorsen's model and DNS was less dependent on Strouhal number than the position of the pitch axis along the chord. Pitching about the mid-chord, while resulting in a smaller Strouhal number than pitching about the leading edge, promotes leading edge separation and dynamic stall effects which are not captured by Theodorsen's model. However, Theodorsen's model doesn't agree with DNS for any pitch point if the angle of attack excursion is large enough to cause periodic vortex shedding. This is an important relationship between the theory for pitching and plunging airfoils; in particular, the theory breaks down in both cases when the angle of attack (resp. effective angle of attack) excursion exceeds the critical stall angle. This observation is supported by the method of indicial response, where agreement between model and data begins to break down for large pitch-up maneuvers. The inability to capture unsteady effects due to high angle of attack is a fundamental limitation of both methods.

The Galerkin projected dynamics onto POD modes for a flat plate at Reynolds number 100 and angle of attack  $\alpha = 30^\circ$  demonstrate the ability of a simple two dimensional ODE model to capture the effects of laminar, periodic vortex shedding. This evidence is supported by similar heuristic models developed for shedding behind a cylinder<sup>23</sup> and behind a low Reynolds number flat plate<sup>24</sup>. While these POD modes and the low order model allow for accurate reconstruction of the flow field and preserve Lagrangian coherent structures, it is not clear that this model is directly useful for reconstructing body forces quickly and accurately, since lift and drag forces depend nonlinearly on the flow field, meaning that contributions from different POD modes cannot be added independently.

There are a number of interesting future directions stemming from this work. First, it is natural to expand the POD analysis and reduced order models to include airfoils in motion. These models promise to extend our capability beyond classical unsteady models in the case of highly agile maneuvers. A parallel investigation would attempt to combine heuristic and Galerkin projected ODE models with the unsteady theory of Theodorsen, allowing for the inclusion of pitch angle and center of mass motion as inputs. A physically motivated model, such as Theodorsen's, which is modified to capture unsteady affects at a fixed high angle of attack will allow for more accurate comparison between ODE model and DNS for complex maneuvers. It will also be interesting to apply balancing techniques, such as balanced POD (BPOD), to provide models which are ideal for observer-based control. However, this theory is limited to linearized models, and will have to be extended to include fully nonlinear unsteady flow fields.

## VI. Acknowledgments

This work was supported by the Air Force Office of Scientific Research, grants FA9550-05-1-0369 and FA9550-07-1-0127.

## References

- <sup>1</sup>Birch, J. and Dickinson, M., "Spanwise flow and the attachment of the leading-edge vortex on insect wings." *Nature*, Vol. 412, 2001, pp. 729–733.
- <sup>2</sup>Sane, S., "The aerodynamics of insect flight." *J. Exp. Biol.*, Vol. 206, No. 23, 2003, pp. 4191–4208.
- <sup>3</sup>Zbikowski, R., "On aerodynamic modelling of an insect-like flapping wing in hover for micro air vehicles," *Phil. Trans. R. Soc. Lond. A*, Vol. 360, 2002, pp. 273–290.
- <sup>4</sup>Videler, J., Samhuis, E., and Povel, G., "Leading-edge vortex lifts swifts." *Science*, Vol. 306, 2004, pp. 1960–1962.
- <sup>5</sup>Smith, A., *Vortex models for the control of stall.*, PhD thesis, Boston University, 2005.
- <sup>6</sup>Magill, J., Bachmann, M., Rixon, G., and McManus, K., "Dynamic stall control using a model-based observer." *J. Aircraft*, Vol. 40, No. 2, 2003, pp. 355–362.
- <sup>7</sup>Ahuja, S., Rowley, C., Kevrekidis, I., Wei, M., Colonius, T., and Tadmor, G., "Low-dimensional models for control of leading-edge vortices: Equilibria and linearized models." *AIAA Aerospace Sciences Meeting and Exhibit*, 2007.
- <sup>8</sup>Ol, M., McAuliffe, B., Hanff, E., Scholz, U., and Kahler, C., "Comparison of laminar separation bubble measurements on a low Reynolds number airfoil in three facilities," *35th AIAA Fluid Dynamics Conference and Exhibit*, 2005.

- <sup>9</sup>Kaplan, S., Altman, A., and Ol, M., “Wake vorticity measurements for low aspect ratio wings at low Reynolds number,” *Journal of Aircraft*, Vol. 44, No. 1, 2007, pp. 241–251.
- <sup>10</sup>Stengel, R., *Flight Dynamics*, Princeton University Press, 2004.
- <sup>11</sup>Theodorsen, T., “General theory of aerodynamic instability and the mechanism of flutter,” Tech. Rep. 496, NACA, 1935.
- <sup>12</sup>Sears, W., “Some aspects of non-stationary airfoil theory and its practical applications,” *AIAA Journal Special Supplement: Centennial of Powered Flight*, Vol. 8, No. 3, 1941, pp. 104–108.
- <sup>13</sup>Wagner, H., “Über die Entstehung des dynamischen Auftriebes von Tragflügeln,” *Zeitschrift für Angewandte Mathematic und Mechanik*, Vol. 5, No. 1, 35 1925, pp. 17.
- <sup>14</sup>Küsner, H., “Zusammenfassender Bericht über den instationären Auftrieb von Flügeln,” *Luftfahrtforschung*, Vol. 13, No. 12, 1935, pp. 410–424.
- <sup>15</sup>Leishman, J. G., *Principles of Helicopter Aerodynamics*, Cambridge University Press, 2nd ed., 2006.
- <sup>16</sup>Chorin, A. and Marsden, J., *A mathematical introduction to fluid mechanics*, Vol. 4 of *Texts in Applied Mathematics*, Springer-Verlag, 1993.
- <sup>17</sup>Holmes, P., Lumley, J., and Berkooz, G., *Turbulence, Coherent Structures, Dynamical Systems and Symmetry*, Cambridge University Press, 1996.
- <sup>18</sup>Taira, K. and Colonius, T., “The immersed boundary method: a projection approach,” *J. Comput. Phys.*, Vol. 225, No. 2, 2007, pp. 2118–2137.
- <sup>19</sup>Colonius, T. and Taira, K., “A fast immersed boundary method using a nullspace approach and multi-domain far-field boundary conditions,” *Comput. Methods Appl. Mech. Engrg.*, Vol. 197, 2008, pp. 2131–2146.
- <sup>20</sup>Haller, G., “Lagrangian coherent structures from approximate velocity data,” *Physics of Fluids*, Vol. 14, No. 6, 2002, pp. 1851–1861.
- <sup>21</sup>Shadden, S., Lekien, F., and Marsden, J., “Definition and properties of Lagrangian coherent structures from finite-time Lyapunov exponents in two-dimensional aperiodic flows,” *Physica D*, Vol. 212, No. 34, 2005, pp. 271–304.
- <sup>22</sup>Rowley, C., “Model reduction for fluids using balanced proper orthogonal decomposition,” *Int. J. Bifurcation Chaos*, Vol. 15, No. 3, 2005, pp. 997–1013.
- <sup>23</sup>Noack, J., Afanasiev, K., Morzynski, M., Tadmor, G., and Thiele, F., “A hierarchy of low-dimensional models for the transient and post-transient cylinder wake,” *J. Fluid Mech.*, Vol. 497, 2003, pp. 335–363.
- <sup>24</sup>Brunton, S., Rowley, C., Taira, K., Colonius, T., Collins, J., and Williams, D., “Unsteady aerodynamic forces on small-scale wings: experiments, simulations and models,” *46th AIAA Aerospace Sciences Meeting and Exhibit*, 2008.
- <sup>25</sup>Taira, K., Dickson, W., Colonius, T., Dickinson, M., and Rowley, C., “Unsteadiness in flow over a flat plate at angle-of-attack at low Reynolds numbers,” *AIAA Aerospace Sciences Meeting and Exhibit*, 2007.
- <sup>26</sup>Taira, K. and Colonius, T., “On the effect of tip vortices in low-Reynolds-number post-stall flow control,” *AIAA Journal*, 2008.
- <sup>27</sup>Taira, K. and Colonius, T., “Three-dimensional flows around low-aspect-ratio flat-plate wings at low Reynolds numbers,” *J. Fluid Mech.*, 2008.
- <sup>28</sup>Green, M., Rowley, C., and Haller, G., “Detection of Lagrangian coherent structures in 3D turbulence,” *J. Fluid Mech.*, Vol. 572, 2007, pp. 111–120.
- <sup>29</sup>Lipinski, D., Cardwell, B., and Mohseni, K., “A Lagrangian analysis of two-dimensional airfoil with vortex shedding,” *J. Phys. A: Math. Theor.*, Vol. 41, 2008.
- <sup>30</sup>Brunton, S. and Rowley, C., “A method for fast computation of FTLE fields,” in preparation.
- <sup>31</sup>Ilak, M. and Rowley, C., “Modeling of transitional channel flow using balanced proper orthogonal decomposition,” *Physics of Fluids*, Vol. 20, 2008.
- <sup>32</sup>Koochesfahani, M. M., “Vortical patterns in the wake of an oscillating airfoil,” *AIAA J.*, Vol. 27, 1989, pp. 1200–1205.
- <sup>33</sup>von Karman, T. and Sears, W., “Airfoil theory for non-uniform motion,” *J. Aeronautical Sciences*, Vol. 5, No. 10, 1938, pp. 379–390.